

Bivariate Galaxy Luminosity Functions in the Sloan Digital Sky Survey

N. M. Ball,^{1,2*} J. Loveday,³ R. J. Brunner,^{1,2} I.K. Baldry⁴ and J. Brinkmann⁵

¹*Department of Astronomy, MC-221, University of Illinois, 1002 West Green Street, Urbana, IL 61801, USA*

²*National Center for Supercomputing Applications, MC-476, University of Illinois, 605 East Springfield Avenue, Champaign, IL 61820, USA*

³*Astronomy Centre, University of Sussex, Falmer, Brighton, BN1 9QJ, UK*

⁴*Department of Physics and Astronomy, Johns Hopkins University, 3400 North Charles Street, Baltimore, MD 21218, USA*

⁵*Apache Point Observatory, PO Box 59, Sunspot, NM 88349, USA*

Accepted xxxx Received xxxx

ABSTRACT

Bivariate luminosity functions (LFs) are computed for galaxies in the Sloan Digital Sky Survey Data Release 3 for a range of galaxy properties, including morphological type assigned by an artificial neural network, inverse concentration index, surface brightness (bivariate brightness distribution), eClass spectral type, reference frame colours, Sérsic index, absolute Petrosian 90% radius, stellar mass and galaxy environment. Several of the parameters are used in this way for the first time. In particular, the sample of 25,915 galaxies classified by Hubble type at the resolution E, S0, Sa ... Sd represents the largest such set in an LF by an order of magnitude. The morphological sample is flux limited to galaxies with $r < 15.9$ while the other bivariate LFs use $r < 17.6$ samples with a median redshift of $z \sim 0.1$. A wealth of detail is seen, with clear variation between the LFs according to absolute magnitude and the second parameter. They are consistent with a early type, bright, concentrated, red population and a late type, faint, less concentrated, blue, star forming population. This idea of bimodality has been explored by others as it suggests two major underlying physical processes. It is considered further in Ball et al. (2005, in preparation) in the context of galaxy colour and morphology. The LF bivariate with surface brightness is fit with the Chołoniewski function (a Schechter function in absolute magnitude and Gaussian in surface brightness) and the fit is found to be poor, as might be expected if the LF is a sum of more fundamental processes whose detail is visible in the dataset.

Key words: cosmology: observations – methods: data analysis – methods: statistical – galaxies: fundamental parameters – galaxies: luminosity function – galaxies: statistics

1 INTRODUCTION

The galaxy luminosity function (LF) is well-known as a fundamental measurement of the properties of galaxies. It constrains theories of their formation and evolution, such as biased galaxy formation and is needed for many other measurements. Examples are the luminosity density in the universe, the selection function in magnitude-limited galaxy surveys, the distances to various types of object, the number of absorbing objects subdivided by redshift and deprojecting the angular correlation function from two dimensions to three.

The general or universal luminosity function, i.e. that for all galaxies, is defined as the comoving number density of galaxies from luminosity L to $L + dL$

$$dN = \phi(L) dL dV. \quad (1)$$

Measurements of the universal form began with Hubble (1936a,b,c), who claimed a Gaussian form. Various studies followed, which included data on dwarf galaxies in clusters (e.g. Abell 1962) and the study of Holmberg (1974) of galaxies in the field. Both of these argued for a power law faint end slope.

In the mid 1970s it was suggested (Schechter 1976) that the optical LF can be approximated by the function

$$\phi(L) dL = \phi^* \left(\frac{L}{L^*} \right)^\alpha \exp \left(-\frac{L}{L^*} \right) d \left(\frac{L}{L^*} \right), \quad (2)$$

where ϕ^* is the normalisation, L^* is the characteristic luminosity above which the function has an exponential cutoff and α is the value of the power-law slope below L^* . The Schechter function, as it is now known, has been used for most subsequent characterisations of the universal LF. The function is motivated by self-similar gravitational condensation of structures (Press & Schechter 1974), except that α is not a fixed parameter.

Until recently the study of the LF, particularly for field galaxies as opposed to those in clusters, has been hampered by the lack

* E-mail: nball@astro.uiuc.edu

of large samples. Few galaxies had redshifts and the photometry was from photographic plates, resulting in a large variation in the measured LF between different surveys. In the past decade data from large redshift surveys, such as the 2dF Galaxy Redshift Survey (2dFGRS) and the Sloan Digital Sky Survey (SDSS) have become available, greatly improving the situation, although the LFs are still not in perfect agreement.

Whilst the universal LF is reasonably well constrained, it is well-known that the LF varies as a function of intrinsic galaxy properties and galaxy environment. Thus the universal LF needs to be augmented by a description of this variation. As above, the lack of data until recently has hampered such studies, but with the large sample sizes (2dFGRS and SDSS) and five band CCD photometry (SDSS) now available, detailed divisions of the galaxies into samples which are still statistically significant is now possible.

Previous studies of non-universal LFs have included those focusing on specific environments, particularly clusters as the galaxies are all at approximately the same distance and in a narrow field of view, those on specific types of galaxies, those which divide the general LF according to some criterion and fit functions to each bin, and those which study the LF bivariate with another parameter, either binned or as an analytical function.

Various theories and simulations exist on the origin of the LF, tied in with the physics of galaxy formation. Examples are Benson et al. (2003) who begin with the mass function of dark matter halos in the Λ CDM cosmology and add gas cooling, photoionization, feedback (e.g. from supernovae), galaxy merging and thermal conduction. Mo et al. (2004) assume that the segregation of the galaxy population by environment is due to that of halo properties and use the halo occupation distribution to give predicted LFs by environment.

Further details of the LF are in various reviews, for example Binggeli, Sandage & Tammann (1988) and subdivided by morphological type in de Lapparent (2003).

In this paper the bivariate LF is studied in bins using the non-parametric stepwise maximum likelihood method of Efstathiou, Ellis & Peterson (1988) and two-dimensional analytical functions are fitted to the results. Previous studies that have done this include Chołoniowski (1985) subdivided by radius, Sodr  & Lahav (1993) subdivided by galaxy diameter and Cross et al. (2001), Cross & Driver (2002) and Driver et al. (2005) subdivided by surface brightness. The latter quantity is also known as the bivariate brightness distribution.

Ball et al. (2004) showed that morphological types can be reliably assigned to galaxies in the SDSS using artificial neural networks (ANNs) provided a representative training set is available. Here types are assigned to the resolution E, S0, Sa, Sb, Sc, Sd and Im for 25,915 galaxies, which represents the largest such set in an LF by an order of magnitude. In Ball et al. (2005, in preparation, hereafter B05) we use these types to study the variation of galaxy morphology and colour with environment.

The bivariate LFs are computed for galaxies in the Sloan Digital Sky Survey Data Release 3 for a range of galaxy properties, including the morphological type described, inverse concentration index, surface brightness, eClass spectral type, reference frame colours, S rsic index, absolute Petrosian 90% radius, stellar mass and galaxy environment. Several of the parameters are used in this way for the first time. The galaxy sample used depends on the parameter, with most samples flux limited to $r < 17.6$. An exception is the morphology, which is limited to $r < 15.9$.

Here the LF is only considered in the wavebands of the SDSS, but there are many studies in other wavebands, including the ultra-

violet (Baldry et al. 2005; Wyder et al. 2005), near-infrared K band (Loveday 2000; Cole et al. 2001; Kochanek et al. 2001; Eke et al. 2004), radio and x-ray.

The datasets considered here are also of low redshift ($z \lesssim 0.3$) and although evolution has been found (Blanton et al. 2003b; Loveday 2004), here the bivariate function is measured for magnitudes K corrected to the mean redshift of the data, which is usually $z \sim 0.1$.

Throughout, the standard spatial geometry is assumed, with Euclidean space, $\Omega_{\text{matter}} = 0.3$ and $\Omega_{\Lambda} = 0.7$. An exception is that the dimensionless Hubble constant, $h = H_0/100 \text{ km s}^{-1} \text{ Mpc}^{-1}$, is taken to be 1 rather than 0.7 for comparability with previous studies such as Blanton et al. (2003b). Absolute magnitudes can be converted by subtracting $5\log h$, which for $h = 0.7$ is -0.77 . Hence h has no effect on the shape of the LF, but it does affect the normalisation.

2 DATA

The SDSS is a project to map π steradians of the northern galactic cap in five bands (u, g, r, i and z) from 3,500–8,900 Å. This will provide photometry for of order 5×10^7 galaxies. A multifibre spectrograph will provide redshifts and spectra for approximately 10^6 of these. A technical summary of the survey is given in York et al. (2000). The imaging camera is described in Gunn et al. (1998). The photometric system and calibration are described in Fukugita et al. (1996), Hogg et al. (2001), Smith et al. (2002) and Ivezi  et al. (2004). The astrometric calibration is in Pier et al. (2003) and the data pipelines are in Lupton et al. (2001), Frieman et al. and Schlegel et al. (in preparation).

The targeting pipeline chooses targets for spectroscopy from the imaging. A tiling algorithm (Blanton et al. 2003) then assigns the spectroscopic fibres to the targets, the main source of incompleteness being the minimum distance of 55 arcsec between the fibres. This causes about 6% of galaxies to be missed, and these will be biased towards regions with a high surface density of galaxies. The algorithm gives a more uniform completeness on the sky than a uniform tiling by taking into account large scale structure, but some bias is still present.

The SDSS galaxies with spectra consist of a ‘main’, flux-limited sample ($r < 17.77$), with a median redshift of 0.104 (Strauss et al. 2002) and a luminous red galaxy sample, approximately volume-limited to $z \approx 0.4$ (Eisenstein et al. 2001). Only the main sample galaxies are used here. The limiting magnitude for the spectra is $r < 17.77$, which is substantially brighter than that for the imaging so the redshift completeness is almost 100%. A typical signal-to-noise value is > 4 per pixel and the spectral resolution is 1800. The redshifts have an RMS accuracy of $\pm 30 \text{ km s}^{-1}$.

This paper uses galaxies from the third data release (DR3, Abazajian et al. 2005) which provides spectra for 374,767 galaxies and photometry for 85 million. The final survey will be approximately 1.5 times this size.

The magnitudes are corrected for galactic reddening using the usual corrections derived from Schlegel, Finkbeiner & Davis (1998). They are K corrected using version 3.2 of the code described in Blanton et al. (2003a). This provides a K correction for each individual galaxy, but does not take into account galaxy evolution or dust. The K corrections were made to the mean redshift of each dataset. The mean was rounded to 0.1 for the sets based on the full main galaxy sample.

2.1 Galaxy Samples and Properties

The absolute magnitude range used was $-24 < M_r < -11$ in 26 bins of 0.5 mag, although the faint of this is undoubtedly incomplete (Blanton et al. 2004). An exception is the JPG morphological type (see below), which was binned in 28 bins of 0.25 mag for $-24 < M_r < -17$. The second parameter in the calculation of each bivariate LF was binned as shown in Table 1. Approximately 20–30 evenly spaced bins were used as this gave a reasonable execution time. The placement of the bins is based on visual inspection, but the value of $\psi(M, X)$ in each bin is independent of the others.

Our analysis allows for the sampling rate of the dataset, which is the ratio of the number of galaxies meeting the criteria for spectra to those which have spectra taken. Here the rate is set at 0.93 due to the 6% incompleteness from the spectroscopic fibres and the rest of the sample being about 99% complete overall (Strauss et al. 2002). The areas used are in Table 1.

For galaxy properties available directly from the SDSS we used the main galaxy sample from DR3, with sample cuts of reddening corrected r -band Petrosian magnitude $r < 17.6$, confidence in spectroscopic redshift $z\text{Conf} > 0.85$ and spectroscopic object class `specClass = GALAXY` (emission line galaxy `GAL_EM` was a placeholder in DR3).

Several groups have calculated derived quantities for galaxies beyond those available in the main survey database. Three of these catalogues have been used here: the New York Value-Added Galaxy Catalog (VAGC, Blanton et al., 2005), the Pittsburgh-Carnegie Mellon Value Added Catalog (VAC; <http://frank.phyast.pitt.edu/dr3/>) and the Japan Participation Group (JPG) catalogue of morphological types. The VAGC gives the Sérsic index, the VAC the absolute Petrosian radius, stellar mass and density environment and the JPG catalogue formed the training set for the neural network morphological types.

The VAGC uses its own data reduction from the raw SDSS data. The galaxies in the VAGC either pass the main sample criteria, slightly modified, are within 2 arcsec of a main sample galaxy, luminous red galaxy or quasar target or are within 2 arcsec of an SDSS spectrum. The dataset used is different to DR3 but comparable in size, with 6,502 square degrees of imaging and 3,836 square degrees of spectroscopy.

The VAC uses DR2 data and the standard SDSS data reduction. It is cross-matched to the original dataset and the 249,725 unique galaxies in the database pass various spectral flags described on the webpage.

Table 1 summarises the galaxy samples, properties and data sources used in the paper, which are now described.

2.2 Neural Network Morphological Types

1875 SDSS galaxies to $r < 15.9$ in the SDSS Early Data Release data (Stoughton et al. 2002) have been classified into morphological types by Nakamura et al. (2003), forming the JPG catalogue. The system used was a modified version of the T-type system (de Vaucouleurs 1959), with the types being assigned in steps of 0.5, with E=0, S0=1, Sa=2, Sb=3, Sc=4, Sd=5 and Im=6.

We have previously shown (Ball et al. 2004) that artificial neural networks (e.g. Bishop 1995; Lahav et al. 1996) are able to assign types to galaxies in the SDSS with an RMS accuracy of 0.5 on this scale, using the JPG catalogue as a training set. This is the same as the spread between the human-classified types by the members of the JPG team. The neural networks are likely to be more objec-

tive than human classifiers would be over the 25,000-galaxy sized sample used here.

We used the same procedures here, updated for DR3 over DR1 and with some modifications. The DR3 was matched to the JPG catalogue using a tolerance of 2 arcseconds and a flux limit of $r < 15.9$. Unassigned types (–1) and galaxies flagged as being likely to have bad photometry were removed as before. In addition, a set of recommended photometric flags, described at <http://www.sdss.org/dr3/>, was applied to select galaxies with clean photometry. After these cuts 1290 galaxies remained. The training and test sets were 645 each with no overlap, from which, as before, galaxies with severely outlying parameters and targets ($> 10\sigma$ from the mean value for the parameter, generally indicative of a measurement error) were iteratively removed for each parameter in turn.

The clean photometry flags were necessary because not all the galaxies to $r < 15.9$ in the whole survey yet have spectra. It was also found that when trained on the full set of 29 parameters in Ball et al. (2004) the types were biased towards early type with increasing redshift to a greater extent than in the JPG catalogue. However, when one trains on the purely morphological subset of the parameters (all those except the magnitudes and colours), the bias is similar to the JPG, reflecting the flux-limited nature of the sample, but the RMS variation between network type and target type is not significantly larger. Hence the latter set is used as the training set here.

The network also has a tendency to ‘avoid the ends of the scale’, resulting in few very late type galaxies and a slight bias away from early type galaxies. This is shown in Fig. 1 of Ball et al. (2004).

2.3 SDSS DR3 Outputs

The concentration index, surface brightness and reference frame colours use Petrosian magnitudes. These measure a constant fraction of the total light and are available in the SDSS in a modified form from that introduced by Petrosian (1976). The Petrosian flux is given by

$$F_P \equiv \int_0^{N_P r_P} 2\pi r' dr' I(r') \quad (3)$$

where r_P is the Petrosian radius, which is the value at which the Petrosian ratio of surface brightnesses

$$R_P(r) \equiv \frac{\int_{0.8r}^{1.25r} 2\pi r' dr' I(r') / [\pi(1.25^2 - 0.8^2)]}{\int_0^r 2\pi r' dr' I(r') / (\pi r^2)} \quad (4)$$

has a certain value, chosen in the SDSS to be 0.2. The number N_P of Petrosian radii within which the flux is measured is equal to 2 in the SDSS. Further details are given in Lupton, Gunn & Szalay (1999) and Stoughton et al. (2002).

The Petrosian radii are not seeing corrected, which causes the surface brightness and concentration to be underestimated for objects of size comparable to the PSF. However the seeing effect is not yet quantified, and there are other approximations such as using a circular as opposed to elliptical aperture and not correcting for dust obscuration. As described in Stoughton et al. (2002) the Petrosian aperture is not missing much flux versus an ideal galaxy light profile, the amount missing being about 20% for a de Vaucouleurs profile and only 1% for an exponential profile. The effect of seeing, which would make the profiles tend towards a PSF, for which 5% of the light is lost, is also small for galaxies in the main sample. Blanton et al. (2003b) show that the resulting luminosity density in

Table 1. Parameters and ranges used in the LFs bivariate with absolute r band magnitude for $-24 < M_r < -11$. See text for further details on the parameters and data sources.

Parameter	Min	Max	Bins	Galaxies	Mag.	Ref. Frame z	Area / deg ²	Data Release	Source
morphological T type	-0.5	6.5	14	1,131	15.9	0.05	230.68	EDR	JPG Catalogue
ANN T type	-0.5	6.5	14	25,915	15.9	0.05	3,732	DR3	ANN morphology
inverse concentration index	0.1	0.7	24	251,744	17.6	0.1	3,732	DR3	SDSS CAS
surface brightness	17	24.5	30	251,739	17.6	0.1	3,732	DR3	SDSS CAS
eClass	-0.6	1	32	251,749	17.6	0.1	3,732	DR3	SDSS CAS
reference frame $u - r$	0	4.25	17	249,342	17.6	0.1	3,732	DR3	SDSS CAS
reference frame $g - r$	-0.25	1.5	28	251,475	17.6	0.1	3,732	DR3	SDSS CAS
reference frame $r - i$	-0.25	1	20	251,492	17.6	0.1	3,732	DR3	SDSS CAS
reference frame $r - z$	-0.5	1.25	28	251,167	17.6	0.1	3,732	DR3	SDSS CAS
Sérsic index	0	6	24	242,058	17.6	0.1	3,836	~ DR3	NYU VAGC
Petrosian 90% radius / kpc	0	50	25	179,875	17.6	0.135	2,627	DR2	Pitt/CMU VAC
$\log(\text{stellar mass}) / M_{\odot}$	6	12	24	175,460	17.6	0.108	2,627	DR2	Pitt/CMU VAC
Σ_5 surface density / M_{pc}^{-2}	0	10	20	35,906	17.6	0.051	2,627	DR2	Pitt/CMU VAC

r is very similar to that from the Sérsic profile, the difference being $j_{0.1}(\text{Sersic}) = j_{0.1}(\text{Petrosian}) - 0.03$. They suggest that the similarity shows that the true luminosity density is also of a similar value.

The inverse concentration index CI_{inv} is then R_{50}/R_{90} where R_{50} and R_{90} are the radii within which 50 and 90 per cent of the Petrosian flux is received. The inverse is used because it has the range 0-1.

Parameters other than magnitudes and colours are measured in the r band, since this band is used to define the aperture through which Petrosian flux is measured for all five bands.

The Petrosian half-light surface brightness used here is given by

$$\mu = m_r + 2.5 \log(2\pi R_{50}^2). \quad (5)$$

m_r is the r band magnitude.

The eClass (Connolly et al. 1995; Connolly & Szalay 1999; Yip et al. 2004) is a continuous one parameter type assigned from the projection of the first three principal components (PCs) of the ensemble of SDSS galaxy spectra. The locus of points forms an approximately one dimensional curve in the volume of PC1, PC2 and PC3. This is a generalization of the mixing angle ϕ in PC1 and PC2

$$\phi = \tan^{-1} \left(\frac{a_2}{a_1} \right), \quad (6)$$

where a_1 and a_2 are the eigencoefficients of PC1 and PC2. The range is from approximately -0.5 (corresponding to early type galaxies) to 1 (late type). The eClass is also robust to missing data in the spectra used for its derivation, and is almost independent of redshift.

The reference frame colours are taken from the K corrected values described above. All ten colours from $ugriz$ were investigated.

2.4 Outputs from additional SDSS Catalogues

The Sérsic profile (Sérsic 1968; Graham & Driver 2005) is obtained by generalising the de Vaucouleurs profile (de Vaucouleurs 1948) to have index $\frac{1}{n}$ instead of $\frac{1}{4}$, giving

$$I(r) = I_0 \exp\{-b_n[(r/r_e)^{1/n}]\}, \quad (7)$$

where b_n is such that half the total luminosity is within r_e . The fitting procedure used in the VAGC is described in Appendix A of Blanton et al. (2003): the axisymmetric Sérsic profile is fitted to the azimuthally averaged galaxy light profile available from the SDSS database. The profiles are corrected for seeing, which is modelled using three axisymmetric Gaussians. Here just the Sérsic index n is used. The de Vaucouleurs and exponential profiles correspond to $n = 4$ and $n = 1$ respectively.

The absolute radius of a galaxy is taken from the VAC, where it is calculated from the apparent Petrosian 90% radius using the concordance Λ CDM cosmology ($\Omega_{\Lambda} = 0.7$, $\Omega_m = 0.3$, $h = 0.7$). The value for the absolute 50% radius is also given.

The VAC includes the quantity `mpa_stellarmass` (Kauffmann et al. 2003), obtained from object matching to the database at the Max Planck Institute for Astrophysics at <http://www.mpa-garching.mpg.de/SDSS/>. The quantity is the log of the median dust-corrected mass in solar units. It is calculated from the stellar mass to light ratio predicted by a large library of models of star formation history.

The VAC contains a measure of galaxy environment as the parameter `density_z002080`. This is the distance to the N th nearest neighbour within $\pm 1000 \text{ km s}^{-1}$ in redshift for $0.02 < z < 0.08$. The slice is used to minimise contamination from interlopers. Galaxies for which the survey edge is reached before the N th nearest neighbour are not included as this would bias the estimated densities downwards near the survey edges. Here $N = 5$, following Balogh et al. (2004) who choose this value to approximate Dressler (1980) who uses $N = 10$ before correction for superimposed galaxies. The surface density of galaxies is then given by $\Sigma_N = N/\pi d_N^2$. The nearest neighbour must be of magnitude $r < 17.7$ at $z = 0.08$, which corresponds to $M_r < -20$, although all galaxies in the sample are given a nearest neighbour measurement. This cut ensures a uniform density measurement over the redshift range of the sample rather than the density decreasing with redshift due to missed faint galaxies.

3 BIVARIATE LUMINOSITY FUNCTIONS

Unlike the univariate LF in which the Schechter function is often used, there is no common functional form for the bivariate LF, so a nonparametric estimator is chosen. We use the popular stepwise

maximum likelihood (SWML) method of Efstathiou et al. (1988), following the extension to a bivariate distribution by Sodr e & Lahav (1993). The maximum likelihood method has well defined error properties (Kendall & Stuart 1961) and in the comparison between LF estimators of Takeuchi et al. (2000) the SWML was shown to be a good estimator.

The SWML gains independence of inhomogeneities in the galaxy distribution by assuming that this is the case via the universal form: $n(L, \mathbf{x}) = \phi(L)\rho(\mathbf{x})$. This means that the $\phi(L)$ shape is independent of its normalisation, which then has to be found separately. The data must also be binned over the ranges of the parameters considered.

Here the bivariate LF is given by $\psi(L, X)$ or $\psi(M, X)$ where X is the second parameter.

For a galaxy which is observable if its luminosity L lies in the range $L_{\min}-L_{\max}$ and X lies in the range $X_{\min}-X_{\max}$ (these limits in general being redshift dependent), the probability of seeing that galaxy with luminosity L_i and $X = X_i$ at redshift z_i is

$$p_i \propto \psi(L_i, X_i) / \int_{L_{\min}(z_i)}^{L_{\max}(z_i)} \int_{X_{\min}(z_i)}^{X_{\max}(z_i)} \psi(L, X) dL dX. \quad (8)$$

The X limits are a function of z if the sample is explicitly or implicitly selected on X . Most samples here are not explicitly selected on X .

The likelihood $\mathcal{L} = \prod p_i$ is then maximised with respect to $\psi(L, X)$. In practice, one maximises the log-likelihood $\ln \mathcal{L} = \sum \ln p_i$.

For the SWML method, the discrete version of this is used. $\psi(M, X)$ is parametrised as the number density of galaxies

$$\psi(M, X) = \psi_{jk} \quad (j = 1 \dots N_M; k = 1 \dots N_X) \quad (9)$$

in N_M and N_X evenly spaced bins in absolute magnitude

$$M_j - \frac{\Delta M}{2} < M < M_j + \frac{\Delta M}{2} \quad (10)$$

and X

$$X_k - \frac{\Delta X}{2} < X < X_k + \frac{\Delta X}{2}. \quad (11)$$

Magnitude bins are preferred to luminosity bins as the distribution is more evenly spread.

The likelihood is then given using the discrete equivalent of equation 8

$$\ln \mathcal{L} = \sum_{i=1}^{N_g} \sum_{j=1}^{N_M} \sum_{k=1}^{N_X} W_{ijk} \ln \psi_{jk} - \sum_{i=1}^{N_g} \ln \left(\sum_{j=1}^{N_M} \sum_{k=1}^{N_X} H_{ijk} \psi_{jk} \right) + \text{constant}, \quad (12)$$

where

$$W_{ijk} = \begin{cases} 1 & \text{if } -\Delta M/2 \leq M_i - M_j \leq \Delta M/2 \\ & \text{and } -\Delta X/2 \leq X_i - X_k \leq \Delta X/2, \\ 0 & \text{otherwise} \end{cases} \quad (13)$$

and

$$H_{ijk} = \frac{1}{\Delta M \Delta X} \times \int_{M-\Delta M/2}^{M+\Delta M/2} \int_{X-\Delta X/2}^{X+\Delta X/2} dM dX O_{ijk}. \quad (14)$$

O_{ijk} is the survey window function at that redshift

$$O_{ijk} = \begin{cases} 1 & \text{if } M_{\min}(z_i) \leq M_j \leq M_{\max}(z_i) \\ & \text{and } X_{\min}(z_i) \leq X_k \leq X_{\max}(z_i) \\ 0 & \text{otherwise.} \end{cases} \quad (15)$$

The constant in (12) is fixed by using a Lagrangian multiplier λ : the constraint

$$g = \sum_j \sum_k \psi_{jk} \Delta M \Delta X - 1 = 0 \quad (16)$$

is applied and the new likelihood $\ln \mathcal{L}' = \ln \mathcal{L} + \lambda g(\psi_{jk})$ is maximised with respect to ψ_{jk} and λ , requiring $\lambda = 0$.

The maximum likelihood estimate $\partial \ln \mathcal{L}' / \partial \psi_{jk} = 0$ is then

$$\psi_{jk} = \frac{\sum_{i=1}^{N_g} W_{ijk}}{\sum_{i=1}^{N_g} [H_{ijk} / \sum_{l=1}^{N_M} \sum_{m=1}^{N_X} \psi_{lm} H_{ilm}]}, \quad (17)$$

where ψ_{lm} is from the previous iteration.

Following Efstathiou et al., the errors on the parameters are estimated using the fact that the MLM estimates ψ_{jk} are asymptotically normally distributed with the covariance matrix

$$\text{cov}(\psi_{jk}) = \mathbf{I}^{-1}(\psi_{jk}), \quad (18)$$

where \mathbf{I} is the information matrix (their equation 2.13b).

For the normalisation, the estimator of the space density \bar{n} of galaxies is

$$f\bar{n} = \sum_{i=1}^{N_{gal}} w(z_i) / \int_{z_{\min}}^{z_{\max}} S(z)w(z) dV, \quad (19)$$

with sampling rate f . The selection function S from L_1 to L_2 is

$$S(z) = \sum_{L'_1}^{L'_2} \sum_{X'_1}^{X'_2} \psi(L, X) / \sum_{L_1}^{L_2} \sum_{X_1}^{X_2} \psi(L, X), \quad (20)$$

where $L'_1 = \max(L_{\min}(z), L_1)$, $L'_2 = \min(L_{\max}(z), L_2)$ and similarly for X . The limits on the sums in the numerator depend on the K correction, which is determined using the average SED for the sample. These limits will in general include partial bins with appropriate weighting due to the summation limits not falling at the edge of a bin.

We use the weighting function

$$w(z) = \frac{1}{[1 + 4\pi f\bar{n}J_3(r_c)S(z)]}, \quad (21)$$

where

$$J_3(r_c) = \int_0^{r_c} r^2 \xi(r) dr, \quad (22)$$

r is the distance and $\xi(r)$ the real space galaxy two point correlation function.

The variance in the correlation function can be estimated using a complex formula which minimises the variance in the function and involves the three and four point correlation functions. These are more difficult to measure than the two point and require a large sample such as the SDSS. The weight function in equation 21 was found to be a good approximation by Hamilton (1993) and is widely used. The function minimises the variance in the estimate of the number density so long as r_c is much less than the survey depth. Here $4\pi J_3 = 32000 h^{-3} \text{ Mpc}^3$, using the $\xi(r)$ from Zehavi et al. (2002) which is given as $\xi(r) = (r/6.1 \pm 0.2 h^{-1} \text{ Mpc})^{-1.75 \pm 0.03}$ for $0.1 h^{-1} \text{ Mpc} \leq r \leq 16 h^{-1} \text{ Mpc}$. The effect of using an incorrect value would be to change the normalisation but not the shape

of the LF, for example Loveday (2004) uses the same values of J_3 and ξ as here and finds that halving J_3 reduces the estimated density by 7%. An update to Zehavi et al. (2002), Zehavi et al. (2004b), has a similar ξ value to that used here.

Equation 19 is solved iteratively as it contains w , which contains \bar{n} . The minimum-variance $w(z)$ is described further in Davis & Huchra (1982) and Hamilton (1993).

4 RESULTS

Despite the use of SDSS database flags in cutting the sample, manual inspection of images of objects from a subsample of the bivariate LF bins showed that a fraction of objects at the faint ends of some of the slices are clearly artifacts, for example HII regions from incorrectly deblended galaxies. The incidence of artifacts is complex, dependent on magnitude and the other LF parameter and would require extensive further investigation to eliminate. Here the LF slice is only plotted in the second and third panels of Figs 1–13 when the number of galaxies corresponding to that point in the slice is greater than 20, with the exception of the JPG morphological types where the cut is 5, because these were manually inspected for outliers by the JPG and so the shot noise becomes the limiting factor.

4.1 Morphological Type

The LF bivariate with the JPG catalogue morphological type obtained here is shown in Fig. 1 as a comparison to that obtained by Nakamura et al. (2003) using the same catalogue. Here the LF shows a shallow faint end slope α and bright M^* for early galaxy types, but the change in shape between the later types is less clear than in Nakamura et al. (2003). However, whilst being drawn from the same catalogue the samples are not completely comparable. A different subset of the EDR galaxies is used here, with 1,131 instead of 1,482; the sample is divided into smaller bins and the normalisation is without the explicit redshift cut used in Nakamura et al. (2003). The number is 1,131 rather than the 1,290 in the ANN training set (§2.2) because this is the subset with spectra.

The neural network types enable the sample to be enlarged to 25,915 galaxies, and the result is shown in Fig. 2. This is the first time the LF with detailed morphology has been calculated for a sample of galaxies of this size. Again the broad trends are confirmed, with the early types appearing Gaussian-like but each slice being consistent with a Schechter function. A problem is that cross-contamination between the types will make them tend toward the overall Schechter LF. As suggested in Nakamura et al. (2003) faint dwarf galaxies, which are less concentrated and will thus look more like later types, may also be a contaminant, but in their data this is not a significant effect.

It may well be the case that the morphological types are intrinsically spread over the RMS of 0.5 T types, so the LFs will be cross-contaminated, however with the large sample here the LF differences are significant, as indicated by the sizes of the error bars.

As described in §2, there are some caveats to the ANN types: the lack of types later than 4.5 is seen; the ANN bias away from very early types may affect the LF for this bin but this probably requires an improved training set to check. If the training set without the clean photometry flags were used, hence leaving in more late type galaxies, the ψ greyscale would extend further right by approximately the width of one of the bins, so the LF for very late types is still not seen.

4.2 Inverse Concentration Index

Various papers (e.g. Shimasaku et al. 2001) have shown that the inverse concentration index R_{50}/R_{90} (CI_{inv}) is correlated with the morphological type, and indeed can be used as a simple classifier. In Fig. 3, the expected broad trend of fainter galaxies being less concentrated is seen. Subdivided by CI_{inv} the LF resembles a Schechter function with a steeper faint end slope for less concentrated galaxies. For the bins outside $0.3 < CI_{inv} < 0.6$ the normalisation is lowered due to lack of galaxies. Subdivided by M_r , the CI_{inv} shows an approximately symmetrical distribution which increasingly gains a peak of more concentrated galaxies at brighter luminosities. The distribution is not obviously bimodal, however. The Petrosian radii used here are not seeing corrected, which causes the inverse concentration to be overestimated for objects of size comparable to the PSF. An improvement would be to use the radii from the Sérsic profile (see §4.6) or an elliptical aperture.

4.3 Surface Brightness

The LF bivariate with the surface brightness (SB) has been investigated by previous authors and is also known as the bivariate brightness distribution (BBD). It is important as it allows one to better quantify selection effects in a survey. A recent investigation is described by Driver et al. (2005) which uses the Millennium Galaxy Catalogue. This goes about one magnitude deeper than the SDSS over a smaller region of sky. The BBD was investigated in the SDSS by Shen et al. (2003). Driver et al. (2005) find a systematic offset to fainter values of the SB in the MGC compared to Shen et al. (2003). This is because the MGC uses a better SB definition involving elliptical isophotes - the Petrosian circular aperture used in the SDSS will systematically overestimate the SB as the semimajor axis of the half-light elliptical aperture is always at least as large, and Blanton et al. (2003b) suggests that the Petrosian aperture is not missing much flux (§2.3). Driver et al. (2005) and Shen et al. (2003) see a broadening of the SB distribution with fainter magnitude. The latter fit Gaussians to the SB in bins and the former fit a bivariate function to the BBD. This is also done here in §5. An improvement in all of these investigations would be to account for the effects of dust, which reddens and dims the light, particularly for edge-on spirals.

Fig. 4 shows the BBD for DR3. Split by μ_{R50} , the LF appears Schechter-like, with a fainter M^* and steeper faint end slope towards fainter surface brightness, as expected, although the brightest bins lack galaxies. Split by M_r , the bright galaxies show a Gaussian distribution about $\mu_{R50} \sim 20.8$, which broadens and becomes fainter with fainter M_r . There is a clear lack of faint high surface brightness or bright low surface brightness galaxies. The faint high surface brightness objects which are present may be galaxy fragments incorrectly deblended by the SDSS photometric pipeline but still present in the main galaxy sample. There is also no bimodality evident, meaning that if the galaxies are divided into one or more populations, as suggested by some of the other measures here such as colour, the surface brightness LF is insensitive to it.

4.4 eClass Spectral Type

Fig. 5 shows the LF bivariate with eClass. The expected trends of the LF for low–high eClass values resembling those for early–late types are seen. The low valued eClasses show a Gaussian-like LF, although there are very few faint early types, and this quickly changes to a Schechter-like function. There is a clear population of

bright galaxies with low eClass which probably correspond to the bright ellipticals. Split by M_r , the pattern suggests two populations in a similar way to the CI_{inv} , with the higher valued one rapidly increasing in fraction from bright to faint M_r .

4.5 Colours

The colours are computed using the database Petrosian magnitudes K corrected to $z = 0.1$, the mean of the sample. The r band shifted to $z = 0.1$ has $\lambda_{\text{eff}} \sim 5600 \text{ \AA}$, similar to the V band. They are preferable to the observed frame colours as the galaxies over the whole range are then more directly comparable. The LF fit implicitly assumes no evolution in the sample. One could take this into account by dividing the sample into redshift bins. All ten colours from *ugriz* were investigated and Figs 6–9 show the LF bivariate with $u - r$, $g - r$, $r - i$ and $r - z$, a representative sample of the results.

In the LF split by colour, the expected trends of a fainter M^* and steeper α for bluer colours are seen. There is a clear lack of faint galaxies with redder colours in all four plots. The panels split by colour show that the LFs are Schechter-like, with a steepening faint end slope with bluer colour and possible upturn at fainter magnitudes, apart from in the bluest bin where the slope is already steep.

The $u - r$ colour is used in other investigations such as Balogh et al. (2004) and Baldry et al. (2004) where the galaxies are clearly divided into two populations using counts in colour and morphology bins, which are fit by Gaussians. This is also done in B05 where $u - r$ is compared to the neural network morphological type. Here when the LF is split by M_r the bimodality is also evident but is less obvious due to the logarithmic scale of the ψ axis. There is a minimum in ψ between the peaks for $-21 < M_r < -18.5$, for example. Some of the faint blue objects may be galaxy fragments, as u is the band most associated with star forming regions, and the top left corner for the other three colours is less populated. The plots for $u - g$, $u - i$ and $u - z$ are qualitatively similar to $u - r$, those for $g - i$ and $g - z$ to $g - r$ and $i - z$ to $r - z$, which suggests no obvious physical process apparent in these colours which has been missed by the four shown. The bimodality in the colour is especially evident in $g - r$, with clear peaks for $-21 < M_r < -16$. The bimodality is less obvious for the colours with the redder magnitudes *riz*, although the peaks still appear to be present, just closer together. Star formation is less prominent in r , i and z .

4.6 Sérsic Index

The bivariate LF is shown in Fig. 10. The Sérsic index n used is from the VAGC and is seeing corrected. As such it should be a better tracer of the morphology of the galaxies in the sample than the CI_{inv} . The trends seen above are seen clearly here: the early type galaxies (high n ; a de Vaucouleurs profile is $n = 4$) show a Gaussian-like LF, which changes smoothly to a faint M^* steep faint end slope for low n ($n = 1$ is the exponential profile). Again few faint early types are seen. In the VAGC the index is not assigned values outside the range plotted. The lower normalisation and decreasing faint end is similar to that for the galaxies in Fig. 2 of ANN type below 0.5.

4.7 Absolute Petrosian 90% Radius

The bivariate LF is shown in Fig. 11. The expected pattern of fainter magnitude and higher normalisation due to larger numbers of galaxies with decreasing radius is seen. There is a clear cutoff with magnitude for a given radius, giving a Gaussian-like LF for all but the smallest size bin, which has a Schechter LF. This suggests that the Schechter LF seen in other plots here is due to the smaller galaxies in a sample. The LF bivariate with Petrosian 50% radius is very similar, but scaled to the smaller radii.

4.8 Other measures

Two further parameters were investigated: the galaxy stellar mass and the Σ_N surface density of galaxies. These are shown in Figs 12 and 13.

The stellar mass is useful as a physical parameter which can be directly compared with simulations. The LF was also calculated using the z band absolute magnitude as well as r because this is a better indicator of the stellar mass of a galaxy due to it being less dominated by short-lived bright stars than the bluer bands. A tight correlation is seen in z between the LF and the stellar mass, with the LF in each bin showing a symmetrical shape of similar Gaussian-with-kurtosis form to that in surface brightness. The LFs using the i and r magnitudes are similar, but with a larger spread on the stellar mass axis. However, these results are expected because the luminosity is used in the calculation of the stellar mass in the first place, as part of the mass to light ratio calculated from the models of star formation history (see Kauffmann et al. 2003). For consistency with the other LFs, the r band is shown.

The Σ_N surface density of galaxies from the VAC is used in the morphology-density relation in B05. The bivariate LF appears to be of very similar form across all surface densities, differing only in normalisation. There is a slight increase of bright galaxies at high density, as expected. There is a faint luminosity cutoff due to the $z > 0.02$ limit on the density in the VAC. The $z < 0.08$ limit does not have a strong effect on the bright luminosity galaxies. The narrow limits make it difficult to fit Schechter functions to check for variation in M^* .

The variation in the LF with density and galaxy spectral type is investigated by Croton et al. (2005), who find that the LF is fitted by a Schechter function over all densities, that the ϕ^* and M^* vary smoothly over the density range but that the faint end slope does not change much. Their normalisation is better however, being by the volume in which galaxies are present in the density bin used. The normalisation here is just the overall for the bivariate LF, so the relative normalisations of the bins is essentially arbitrary. This is also seen in the LF divided by M_r , in which one expects less galaxies at low density with normalisation weighted by volume.

It is also possible that the broad lack of change in the shape of the LF with density is related to the similar lack of change in slope in the correlation function divided by luminosity seen by e.g. Connolly et al. (2002) and Zehavi et al. (2002), but this would require further investigation, especially now that Zehavi et al. (2004a) describes departures from the power law.

5 FUNCTION FITTING TO THE BIVARIATE LF

The Schechter function (equation 2) can, by taking $L/L^* = 10^{0.4(M^* - M)}$, be written as

$$\phi(M) dM = 0.4 \ln(10) \phi^* \times \exp[-10^{0.4(M^* - M)}] [-10^{0.4(M^* - M)}]^{\alpha+1} dM. \quad (23)$$

If one then applies Bayes' theorem to the bivariate function then it can be written as

$$\psi(M, X) dM dX = \phi(M) \varphi(X|M) dM dX, \quad (24)$$

which gives two dimensional functions to fit to the SWML estimate. In general any well-behaved function can be fitted, expressed using either side of equation 24.

One choice is to use a Schechter function for $\phi(M)$ and a Gaussian with mean $A(M - M^*) + B$ where A and B are constants for $\varphi(X|M)$. This was first used by Chołoniewski (1985) and is known as the Chołoniewski function:

$$\varphi(X|M) dM dX = \frac{1}{\sqrt{2\pi\sigma_X^2}} \times \exp\left[\frac{-(X - A(M - M^*) - B)^2}{2\sigma_X^2}\right] dM dX. \quad (25)$$

This gives a 6-parameter fit. Chołoniewski (1985) actually used M rather than $M - M^*$ but the latter scales better with the data.

The Chołoniewski function is a Schechter-Gaussian (S-G). One could also fit S-S, G-S or G-G, or use other functions such as a double power-law or a polynomial. The latter would be written in the $\psi(M, X)$ form as this is the easiest way to include the cross-terms.

Due to this greater dimensionality than the univariate LF, a simple maximum likelihood fit is impractical, as the parameter space to explore is large. The method adopted here is the simplex search, which, while not of the greatest accuracy near the minimum, is robust to starting conditions and finds the minimum rapidly.

Here the Matlab implementation, known as `fminsearch`, is used. It implements the Nelder-Mead simplex algorithm (Nelder & Mead 1965) using the method of Lagarias et al. (1998) as described at <http://www.mathworks.com/>. Options used were the Matlab default tolerance of 10^{-4} and a maximum number of iterations of 10000. The search can sometimes become stuck, for example, if the simplex decays to a lower number of dimensions due to the new point being too close to the centroid. However if the search converged it did so in less than this number of iterations.

The measure of goodness of fit, the error function, is the standard χ^2 , given by

$$\chi^2 = \left(\frac{\psi_{obs} - \psi_{fit}}{\overline{\psi_{err}}} \right)^2. \quad (26)$$

The fit is done to $\log_{10}\psi$ rather than ψ so the error is estimated using

$$\overline{\psi_{err}} = \frac{1}{2} [\log_{10}(\psi_{obs} + \psi_{err}) - \log_{10}(\psi_{obs} - \psi_{err})], \quad (27)$$

with ψ_{err} from the information matrix determined as described above.

6 FUNCTION FITTING RESULTS

It was generally found that the functions are a poor fit to the data, as the deviation of the data from a smooth function is large compared to the size of the error bars, giving a large χ^2 . Fig. 14 shows the fit of the Chołoniewski function to the BBD and Fig. 15 the χ^2 values. The fit is particularly poor for bright galaxies around $M_r \sim -22$ and $\mu_{R50} \sim 20$ as the distribution narrows and the number of bright galaxies drops away rapidly with increasing surface brightness. The best fit parameters are $\phi^* = 0.0017$, $M^* = -21$, $\alpha = -1.3$, $\sigma_{\mu_{R50}} = 0.79$, $A = 0.094$, $B = 21$.

Driver et al. (2005) also find a poor fit, but for faint galaxies. They suggest that this is due to the assumption of a constant width for the Gaussian in surface brightness whereas in fact the distribution broadens at fainter values. The linear relation between the mean of the Gaussian and M may also be a factor. It is unlikely that the simplex is always getting stuck in a local minimum far from the global minimum as the fit is poor from a variety of starting points. One could add further parameters but six is already a fair number. The results here are consistent with the constant Gaussian width approximation also being the problem. We confirm the suggestion of Driver et al. (2005) that bulge to disk decomposition is needed.

It is possible that no simple function will provide a good fit, as the superposition of underlying processes generating the bivariate LF may be too complex at the level of precision now available from the data. Or it may be the case that a single function will not fit, but the sum of two or more, each of which describes a different population, for example the red and blue indicated above, may provide a better fit.

Other bivariate LFs such as that with eClass were investigated with S-G and G-G but the fit was also found to be poor. A skew-Gaussian was also tried using an available Matlab port of the software described at <http://azzalini.stat.unipd.it/SN/>. The skew-Gaussian is given by

$$f(x) = 2\phi(x)\Phi(\alpha x), \quad (28)$$

where $\phi(x)$ is the ordinary Gaussian and $\Phi(\alpha x)$ adds the skewness α

$$\phi(x) = \exp(-x^2/2)/\sqrt{2\pi} \quad \Phi(\alpha x) = \int_{-\infty}^{\alpha x} \phi(t) dt. \quad (29)$$

A skewness of $\alpha = 0$ corresponds to the ordinary Gaussian, and a negative α gives the same shape as the positive but reflected about the vertical at $x = 0$. The fits obtained were very similar to those for the ordinary Gaussian, with the skewness tending to low values of order 0.01.

7 DISCUSSION

Two main issues are apparent from the bivariate LF plots presented: that of the bimodality of the galaxy population and whether the underlying LFs per galaxy type are Schechter, Gaussian or some other form.

Concerning a bimodal population, the LFs are consistent with an early type, bright, concentrated, red population and a late type, faint, less concentrated, blue, star forming population. This idea of bimodality has been explored by others as it suggests two major underlying physical processes. It is considered further by B05 in the context of galaxy colour and morphology.

Several results support the idea that the underlying LFs of the giant galaxies, i.e. the usual E, S0 and spirals are Gaussian, whereas those for the dwarfs are Schechter. Sandage, Binggeli & Tammann

(1985) and Jerjen & Tammann (1997) study the cores of nearby clusters, de Lapparent (2003) reviews the LFs subdivided by morphology in various surveys and de Lapparent et al. (2003) focusses on the ESO-Sculptor survey. A physical model supporting the idea is given in Schaeffer & Silk (1988) in which the maximum galaxy mass is limited by baryonic cooling within a dynamical timescale and a minimum mass is given by the minimum virial temperature required for cooling to occur. This gives the Gaussian LF for giants and gas stripping then gives the Schechter function for dwarfs.

The question is whether the LFs are as they appear, with mostly Schechter-like functions, or whether the underlying types are Gaussian, appearing Schechter because type mixing makes the functions tend towards the overall LF, which is Schechter. The idea has previously been discussed in terms of the Hubble morphological types and the effects can be seen here, particularly in Fig. 2. The LF for the early types could either be Schechter or Gaussian with a faint end slope contaminated by dwarfs. In their sample which is essentially a subset of the one used here, Nakamura et al. (2003) use the concentration index to show that the sample is not contaminated with faint galaxies with soft cores, which will be dwarfs. Their concentration index LF is similar to their Hubble type LF. The same is seen here.

The bimodality suggests that concentrated, early spectral type, red, high Sérsic index galaxies correspond to the early morphological types. If this is the case then the Gaussian LF idea is also consistent with the LF plots bivariate with concentration index, eClass, reference frame colours and Sérsic index. These all show LFs for the early types which could be Gaussian with a rise at faint magnitudes, rising to a Schechter function for later types. The trend is particularly clear for the Sérsic index. The idea is also supported by the LF bivariate with absolute Petrosian radius, which shows Gaussian LFs except for those below 10 kpc which are Schechter. The greyscale then suggests that the Schechter form is a result of the galaxies in the under 2 kpc bin. Some of the galaxies in this bin may be incorrectly deblended fragments and so should be investigated further but the LF in this bin still contains over 150 objects. Whatever processes cause the bimodality do not, however, show up in the LF subdivided by surface brightness.

Functions were fitted to the individual LF slices, including Schechter, Gaussian, dual power law Schechter and a sum of two Schechters but the fits were all found to be poor, with $\chi^2/\nu \sim 10$ or more.

As well as the ideas here, further possible followup work includes finding the completeness in each bin rather than assuming uniform completeness over the survey, taking into account the differing density volumes for the LF subdivided by galaxy environment, correcting for dust obscuration, galaxy inclination, seeing and flux missed by the Petrosian aperture, adding further galaxy parameters, including from other datasets, investigating multivariate LFs, fitting further functional forms, extending to higher redshift and comparing to theory via simulations, for example those which use the conditional LF (the LF given the dark halo mass) to populate dark matter haloes with galaxies.

8 CONCLUSIONS

The conclusions of this paper are as follows.

The luminosity function is measured bivariate with various galaxy properties from the SDSS and its associated value-added catalogues. The properties are eyeball morphological type, neural

network morphological type, inverse concentration index CI_{inv} , half-light surface brightness, eClass PCA spectral type, the reference frame colours $u-r$, $g-r$, $r-i$ and $r-z$, the Sérsic index of the light profile, the absolute Petrosian 90% radius of the galaxy, the stellar mass and the Σ_5 surface density of galaxies. Several of the parameters plotted here are new in the context of a bivariate LF, and for those that have previously been studied, the trends seen are confirmed at high signal-to-noise. This is the largest number of parameters studied in one framework for a bivariate LF.

The SDSS is the best dataset currently available for this work, and the large sample combined with CCD photometry is ideal for precision bivariate LFs, enabling division of the galaxy population into numerous smaller samples, each of which is still highly statistically significant. In addition, the stepwise maximum likelihood estimator used is well-known and has been shown to be a good estimator. The magnitudes are K corrected for each individual galaxy using the well-tested K correct code written for the SDSS by Blanton et al. (2003a).

The variation of the LF with all of the parameters is highly significant, both in shape and normalisation, except for Σ_5 where the LF does not change significantly in shape and the normalisation is arbitrary.

The bivariate LFs are consistent with an early type, bright, concentrated, red population and a late type, faint, less concentrated, blue, star forming population. This idea of bimodality has been explored by others as it suggests two major underlying physical processes. It is considered further in B05 in the context of galaxy colour and morphology.

The various morphological measures are consistent, with the Sérsic index showing the same broad trends as the CI_{inv} and neural network morphological type.

The overall patterns of the LFs in the four colours $u-r$, $g-r$, $r-i$ and $r-z$ are similar, as are those for the other six from the SDSS $ugriz$ bands. The main physical change is the increased star formation in the bluer bands.

The LF bivariate with absolute galactic radius shows a Gaussian form except for galaxies below a radius of a few kpc, for which the LF is Schechter. The LF bivariate with galaxy stellar mass shows a tight correlation of higher mass for brighter magnitude, with Gaussian LFs, as expected as the luminosity is used in the calculation of the stellar mass.

The LF bivariate with Σ_5 surface density of galaxies shows little variation in shape over a large range in density from that in a cluster core to the field, being of Schechter function form throughout. Further work would be needed to quantify the variation that is seen.

No definitive conclusion is reached as to whether the underlying LFs for individual types are Gaussian or Schechter, due to the possibility of type mixing. This is particularly prominent in the LFs bivariate with eyeball morphological type assigned by the neural network, as those for the normal galaxies E, S0, and spirals might be expected to be Gaussian but if type mixing is present this causes them to tend towards the overall LF, which is well fit by a Schechter function. The idea is supported by the LFs bivariate with absolute galactic radius and to a lesser extent by Sérsic index, concentration index, spectral type and colours (the bimodality suggests that these correspond to similar galaxy populations). However, the plots are also consistent with Schechter functions with more or less steeply declining faint end slopes, the dwarfs are not obviously significant and they were thought not to be significant in Nakamura et al. (2003), of which this data is essentially a superset.

It may be that the morphology is an intrinsically ‘fuzzy’ mea-

sure, so that the Gaussian LFs will not be seen. However, the contamination may be from dwarf galaxies so an important step is to separate these from the normal galaxies and determine their LF separately. The LF by absolute galactic radius is a step towards this but the next step should be using the azimuthally averaged light profiles available for all galaxies in the SDSS. Similarly, much further detailed investigation would be required to see to what extent the faint end upturns seen in some of the LF slices are real.

Some of the LFs are fitted with analytical functions, which are generally poor fits, probably due to this detail being beyond that reproducible by a simple function. An example is the fit of the Chołoniewski function to the bivariate brightness distribution in which the fit may need to also allow for a variation in the width of the Gaussian with surface brightness, and a possibly nonlinear relation between mean absolute magnitude and mean surface brightness, which results in the addition of two parameters to the six already present. The poor fit is also seen in Driver et al. (2005), where it is interpreted in terms of the diverging trends of bulges and disks with decreasing surface brightness. The fitting method used is easily extended to any of the other bivariate LFs presented here.

ACKNOWLEDGMENTS

Nick Ball thanks Osamu Nakamura for useful discussion on the JPG catalogue and Chris Miller and Michael Balogh for help with the VAC catalogue.

Nick Ball was funded by a PPARC studentship. NMB and RJB would like to acknowledge support from NASA through grants NAG5-12578 and NAG5-12580 as well as support through the NSF PACI Project.

Funding for the creation and distribution of the SDSS Archive has been provided by the Alfred P. Sloan Foundation, the Participating Institutions, the National Aeronautics and Space Administration, the National Science Foundation, the U.S. Department of Energy, the Japanese Monbukagakusho, and the Max Planck Society. The SDSS Web site is <http://www.sdss.org/>.

The SDSS is managed by the Astrophysical Research Consortium (ARC) for the Participating Institutions. The Participating Institutions are The University of Chicago, Fermilab, the Institute for Advanced Study, the Japan Participation Group, The Johns Hopkins University, the Korean Scientist Group, Los Alamos National Laboratory, the Max-Planck-Institute for Astronomy (MPIA), the Max-Planck-Institute for Astrophysics (MPA), New Mexico State University, University of Pittsburgh, University of Portsmouth, Princeton University, the United States Naval Observatory, and the University of Washington.

REFERENCES

- Abazajian K., et al., 2005, *AJ*, 129, 1755
 Abell G. O., 1962, in *IAU Symp. 15: Problems of Extra-Galactic Research Membership of Clusters of Galaxies*. pp 213–+
 Baldry I. K., Glazebrook K., Brinkmann J., Ivezić Ž., Lupton R. H., Nichol R. C., Szalay A. S., 2004, *ApJ*, 600, 681
 Baldry I. K., Glazebrook K., Budavári T., Eisenstein D. J., Annis J., Bahcall N. A., Blanton M. R., Brinkmann J., Csabai I., Heckman T. M., Lin H., Loveday J., Nichol R. C., Schneider D. P., 2005, *MNRAS*, 358, 441
 Ball N. M., Loveday J., Fukugita M., Nakamura O., Okamura S., Brinkmann J., Brunner R. J., 2004, *MNRAS*, 348, 1038
 Balogh M. L., Baldry I. K., Nichol R., Miller C., Bower R., Glazebrook K., 2004, *ApJL*, 615, L101
 Benson A. J., Bower R. G., Frenk C. S., Lacey C. G., Baugh C. M., Cole S., 2003, *ApJ*, 599, 38
 Binggeli B., Sandage A., Tammann G. A., 1988, *ARA&A*, 26, 509
 Bishop C. M., 1995, *Neural Networks for Pattern Recognition*. Oxford University Press, Oxford
 Blanton M. R., Eisenstein D. J., Hogg D. W., Schlegel D. J., Brinkmann J., 2003, Preprint, astro-ph/0310453
 Blanton M. R., et al., 2003a, *AJ*, 125, 2348
 Blanton M. R., et al., 2003b, *ApJ*, 592, 819
 Blanton M. R., et al., 2005, *AJ*, 129, 2562
 Blanton M. R., Lin H., Lupton R. H., Maley F. M., Young N., Zehavi I., Loveday J., 2003, *AJ*, 125, 2276
 Blanton M. R., Lupton R. H., Schlegel D. J., Strauss M. A., Brinkmann J., Fukugita M., Loveday J., 2004, Preprint, astro-ph/0410164
 Chołoniewski J., 1985, *MNRAS*, 214, 197
 Cole S., et al., 2001, *MNRAS*, 326, 255
 Connolly A. J., et al., 2002, *ApJ*, 579, 42
 Connolly A. J., Szalay A. S., 1999, *AJ*, 117, 2052
 Connolly A. J., Szalay A. S., Bershadsky M. A., Kinney A. L., Calzetti D., 1995, *AJ*, 110, 1071
 Cross N., Driver S. P., 2002, *MNRAS*, 329, 579
 Cross N., et al., 2001, *MNRAS*, 324, 825
 Croton D. J., et al., 2005, *MNRAS*, 356, 1155
 Davis M., Huchra J., 1982, *ApJ*, 254, 437
 de Lapparent V., 2003, *A&A*, 408, 845
 de Lapparent V., Galaz G., Bardelli S., Arnouts S., 2003, *A&A*, 404, 831
 de Vaucouleurs G., 1948, *Annales d'Astrophysique*, 11, 247
 de Vaucouleurs G., 1959, *Handbuch der Physik*, 53, 275
 Dressler A., 1980, *ApJ*, 236, 351
 Driver S. P., Liske J., Cross N. J. G., De Propriis R., Allen P. D., 2005, *MNRAS*, 360, 81
 Efsthathiou G., Ellis R. S., Peterson B. A., 1988, *MNRAS*, 232, 431
 Eisenstein D. J., et al., 2001, *AJ*, 122, 2267
 Eke V. R., Baugh C. M., Cole S., Frenk C. S., King H. M., Peacock J. A., 2004, Preprint: astro-ph/0412049
 Fukugita M., Ichikawa T., Gunn J. E., Doi M., Shimasaku K., Schneider D. P., 1996, *AJ*, 111, 1748
 Graham A. W., Driver S. P., 2005, *PASA*, 22, 118
 Gunn J. E., et al., 1998, *AJ*, 116, 3040
 Hamilton A. J. S., 1993, *ApJ*, 417, 19
 Hogg D. W., Finkbeiner D. P., Schlegel D. J., Gunn J. E., 2001, *AJ*, 122, 2129
 Holmberg E., 1974, *Arkiv for Astronomi*, 5, 305
 Hubble E. P., 1936a, Yale University Press
 Hubble E. P., 1936b, *ApJ*, 84, 158
 Hubble E. P., 1936c, *ApJ*, 84, 270
 Ivezić Ž., et al., 2004, *Astronomische Nachrichten*, 325, 583
 Jerjen H., Tammann G. A., 1997, *A&A*, 321, 713
 Kauffmann G., et al., 2003, *MNRAS*, 341, 33
 Kendall M. G., Stuart A., 1961, *The Advanced Theory of Statistics*. Vol. 2, Griffin & Griffin, London
 Kochanek C. S., Pahre M. A., Falco E. E., Huchra J. P., Mader J., Jarrett T. H., Chester T., Cutri R., Schneider S. E., 2001, *ApJ*, 560, 566
 Lagarias J., Reeds J. A., Wright M. H., Wright P. E., 1998, *SIAM Journal of Optimization*, 9, 112

- Lahav O., Naim A., Sodr e L., Storrie-Lombardi M. C., 1996, MNRAS, 283, 207
 Loveday J., 2000, MNRAS, 312, 557
 Loveday J., 2004, MNRAS, 347, 601
 Lupton R. H., Gunn J. E., Ivezi c Z., Knapp G. R., Kent S., Yasuda N., 2001, in ASP Conf. Ser. 238: Astronomical Data Analysis Software and Systems X The SDSS Imaging Pipelines
 Lupton R. H., Gunn J. E., Szalay A. S., 1999, AJ, 118, 1406
 Mo H. J., Yang X., van den Bosch F. C., Jing Y. P., 2004, MNRAS, 349, 205
 Nakamura O., Fukugita M., Yasuda N., Loveday J., Brinkmann J., Schneider D. P., Shimasaku K., SubbaRao M., 2003, AJ, 125, 1682
 Nelder J. A., Mead R., 1965, Computer Journal, 7, 308
 Petrosian V., 1976, ApJL, 209, L1
 Pier J. R., Munn J. A., Hindsley R. B., Hennessy G. S., Kent S. M., Lupton R. H., Ivezi c Z., 2003, AJ, 125, 1559
 Press W. H., Schechter P., 1974, ApJ, 187, 425
 Sandage A., Binggeli B., Tammann G. A., 1985, AJ, 90, 1759
 Schaeffer R., Silk J., 1988, A&A, 203, 273
 Schechter P., 1976, ApJ, 203, 297
 Schlegel D. J., Finkbeiner D. P., Davis M., 1998, ApJ, 500, 525
 S ersic J. L., 1968, Atlas de galaxias australes. Cordoba, Argentina: Observatorio Astronomico, 1968
 Shen S., Mo H. J., White S. D. M., Blanton M. R., Kauffmann G., Voges W., Brinkmann J., Csabai I., 2003, MNRAS, 343, 978
 Shimasaku K., et al., 2001, AJ, 122, 1238
 Smith J. A., et al., 2002, AJ, 123, 2121
 Sodr e L. J., Lahav O., 1993, MNRAS, 260, 285
 Stoughton C., et al., 2002, AJ, 123, 485
 Strauss M. A., et al., 2002, AJ, 124, 1810
 Takeuchi T. T., Yoshikawa K., Ishii T. T., 2000, ApJS, 129, 1
 Wyder T. K., et al., 2005, ApJL, 619, L15
 Yip C. W., et al., 2004, AJ, 128, 585
 York D. G., et al., 2000, AJ, 120, 1579
 Zehavi I., et al., 2002, ApJ, 571, 172
 Zehavi I., et al., 2004a, ApJ, 608, 16
 Zehavi I., et al., 2004b, Preprint, astro-ph/0408569

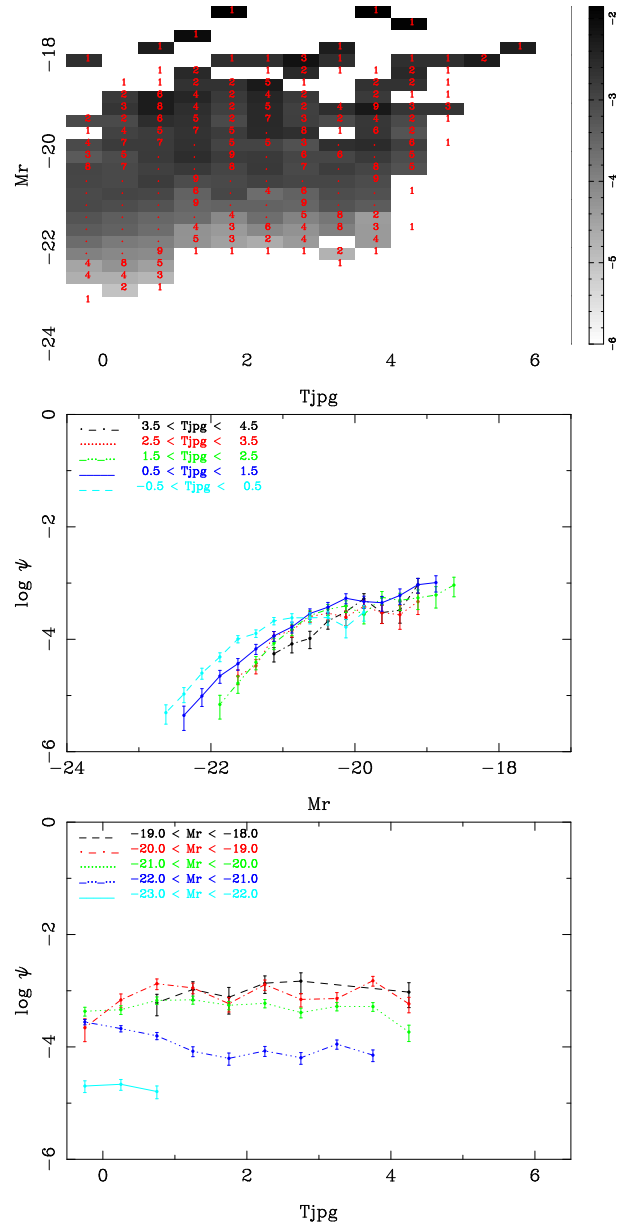


Figure 1. LF bivariate with JPG catalogue morphological type. The greyscale shows the value of $\log_{10}\psi(M, X)$, the LF bivariate with parameter X in each bin, darkening for higher values. The second panel shows vertical slices of $\psi(M, X)$ subdivided by X for the ranges given and the lower panel shows the horizontal slices $\psi(M, X)$ subdivided by M_r . Although the greyscale shows all galaxies, a point appears for the slice only if created by five or more galaxies, as Poisson fluctuations make the slices noisy. In the rest of the LF plots (Figs 2–13) this is increased to twenty (see text). Here X is the JPG type. The red numbers are the number of galaxies in the bin if less than 10, replaced with a red dot for more than 10 and blank for no galaxies. The errors are from the inverse of the information matrix (see text). The expected trend of bright M^* with shallow faint end slope to dim M^* with steep faint end slope with increasing T_{JPG} is seen. Note that for clarity the axes in this figure differ from subsequent figures.

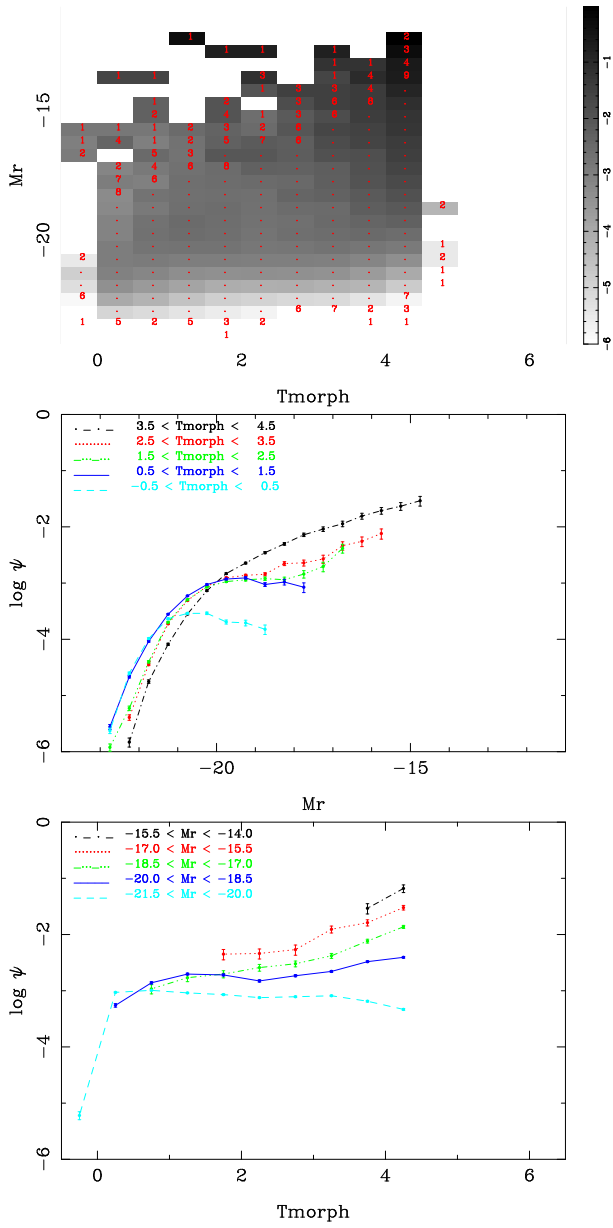


Figure 2. As Fig. 1 but for the neural network morphological type. The trends in Fig. 1 are confirmed, but for 25915 galaxies rather than 1131.

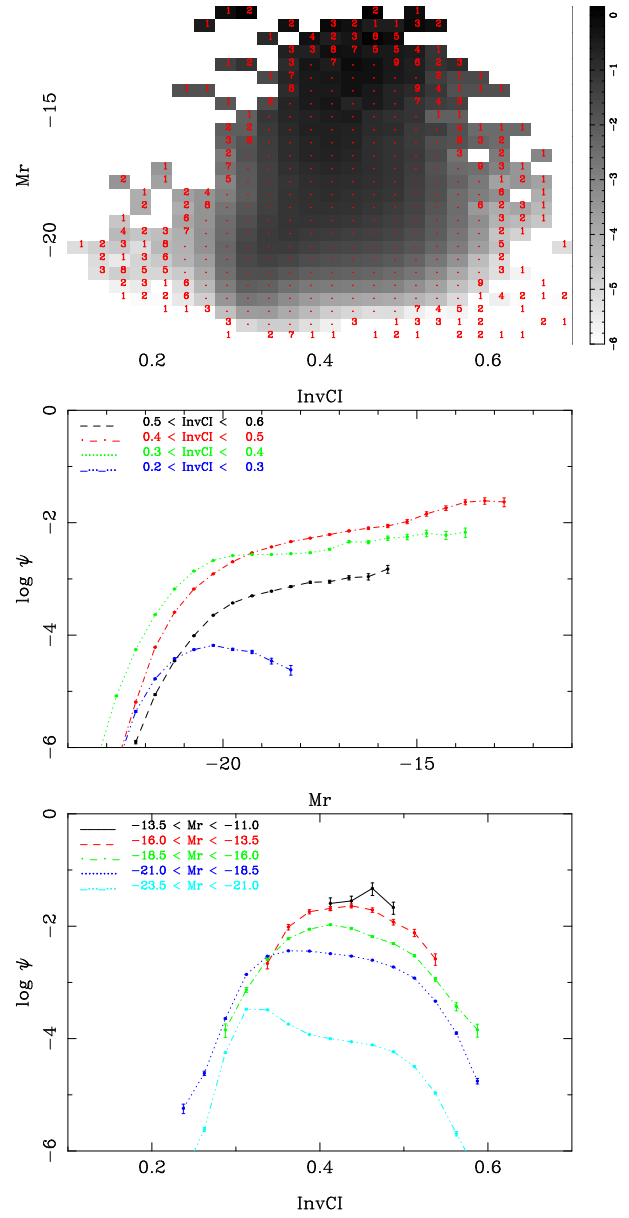


Figure 3. LF bivariate with Petrosian R_{50}/R_{90} inverse concentration index. The expected trend of fainter galaxies being less concentrated is seen, but since the result is based on 251,744 galaxies (see Table 1), much further detail is visible (see text).

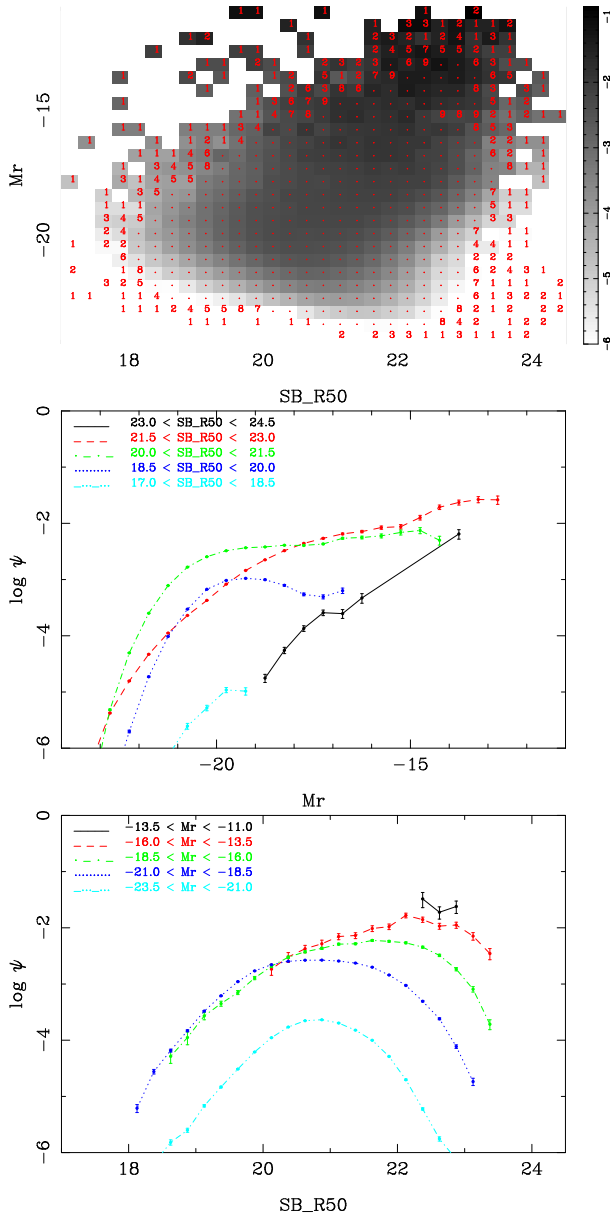


Figure 4. LF bivariate with Petrosian 50% light radius surface brightness. The Petrosian radii are not seeing corrected. The distribution lacks bimodality and confirms the trend of fainter galaxies having lower surface brightness.

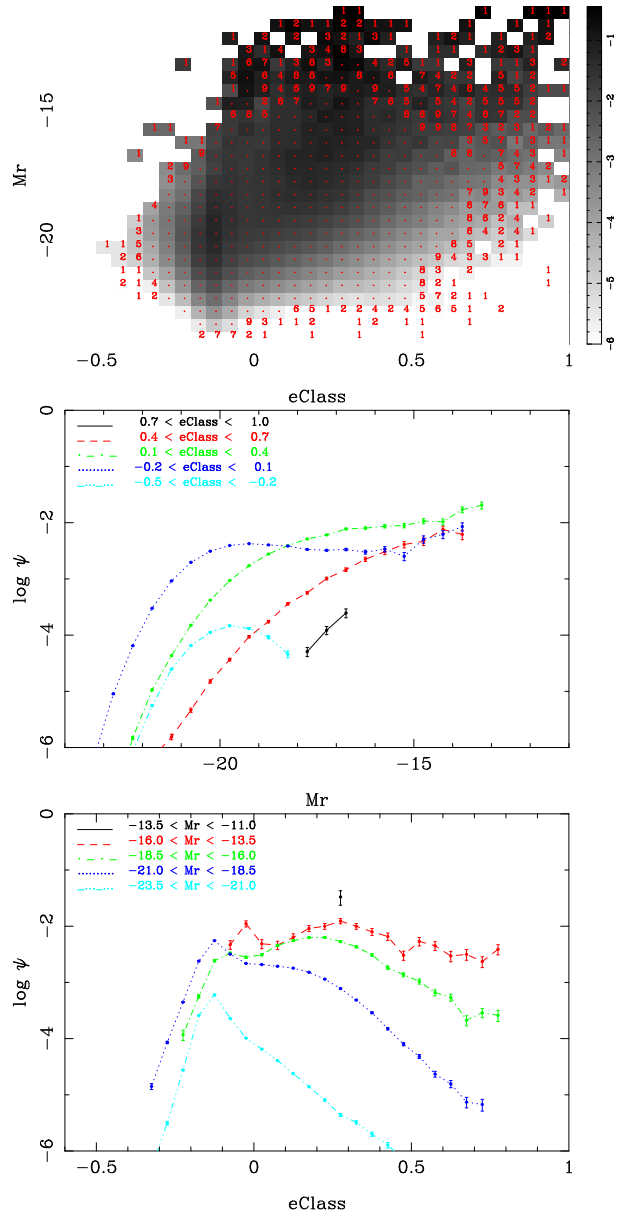


Figure 5. LF bivariate with eClass PCA spectral type. There is a clear population of bright galaxies with low eClass which probably correspond to bright ellipticals. Some bimodality is evident.

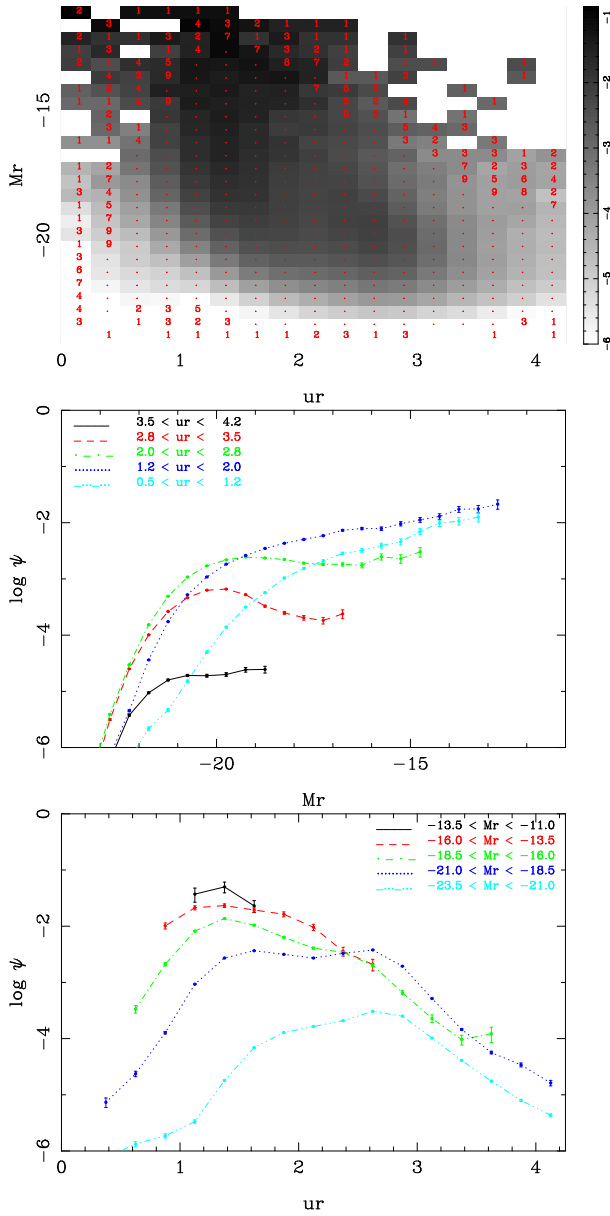


Figure 6. LF bivariate with $u - r$ colour, extinction and K corrected to $z = 0.1$. The expected trends of a fainter M^* and steeper α for bluer colours are seen. Bimodality is present.

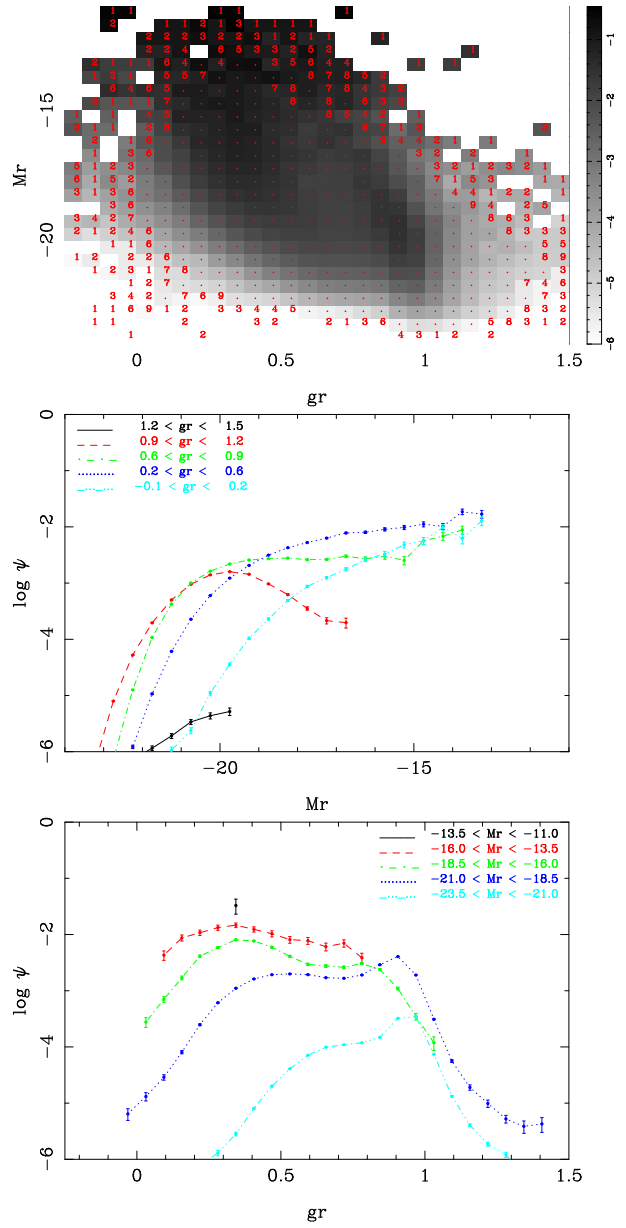


Figure 7. As Fig. 6 but for $g - r$ colour. The results are qualitatively similar to $u - r$ with the red galaxy peak gaining strength.

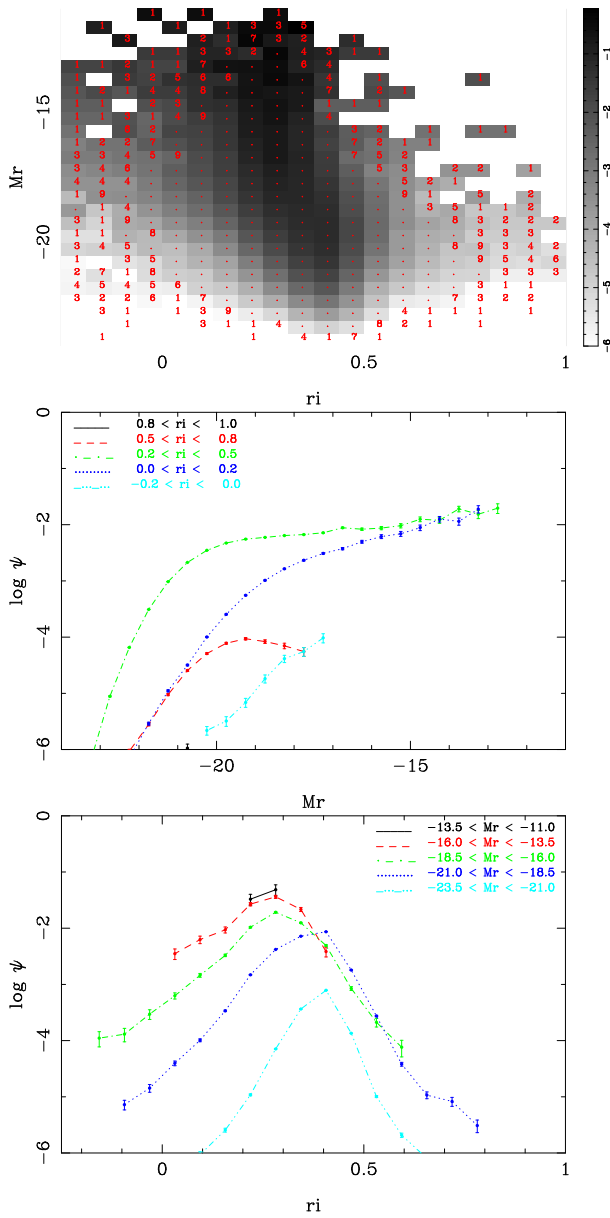


Figure 8. As Fig. 6 but for $r - i$ colour. The blue of star formation is less pronounced.

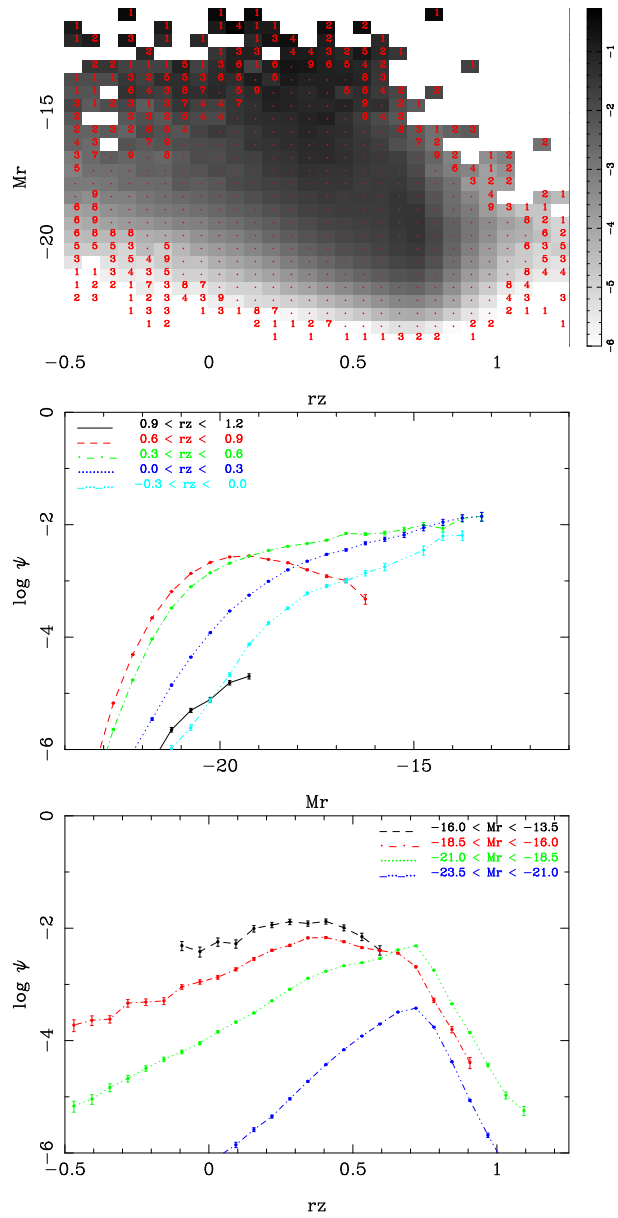


Figure 9. As Fig. 6 but for $r - z$ colour. Bimodality is still seen.

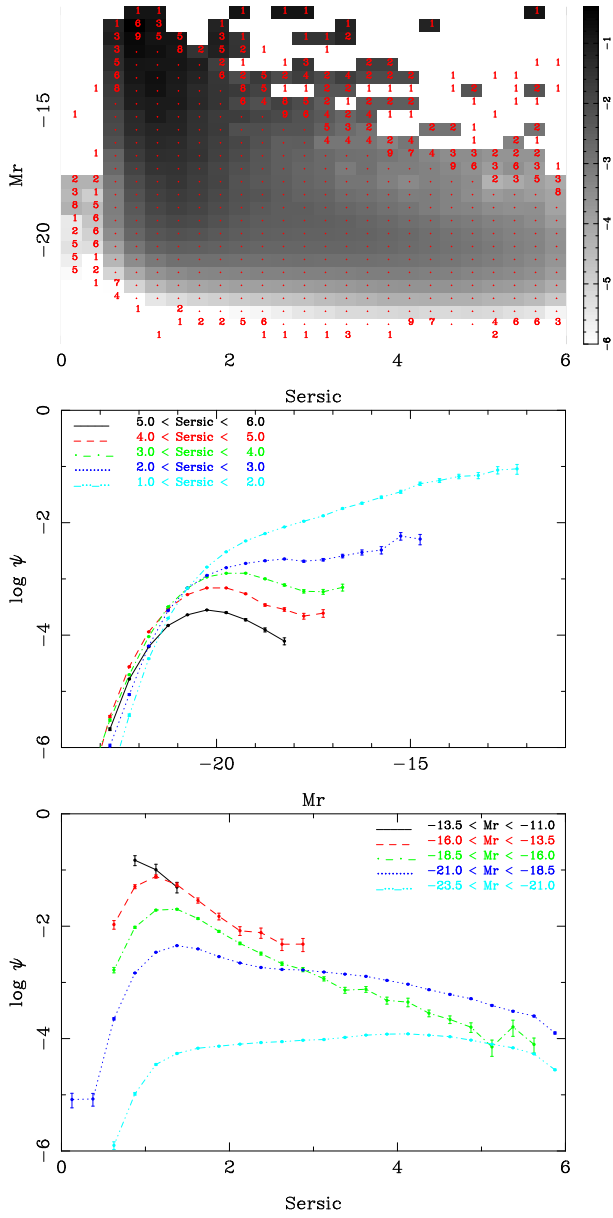


Figure 10. LF bivariate with seeing-corrected Sérsic index n . The Gaussian-like LF for the galaxies of high, n , corresponding to early morphological type, is clearly seen.

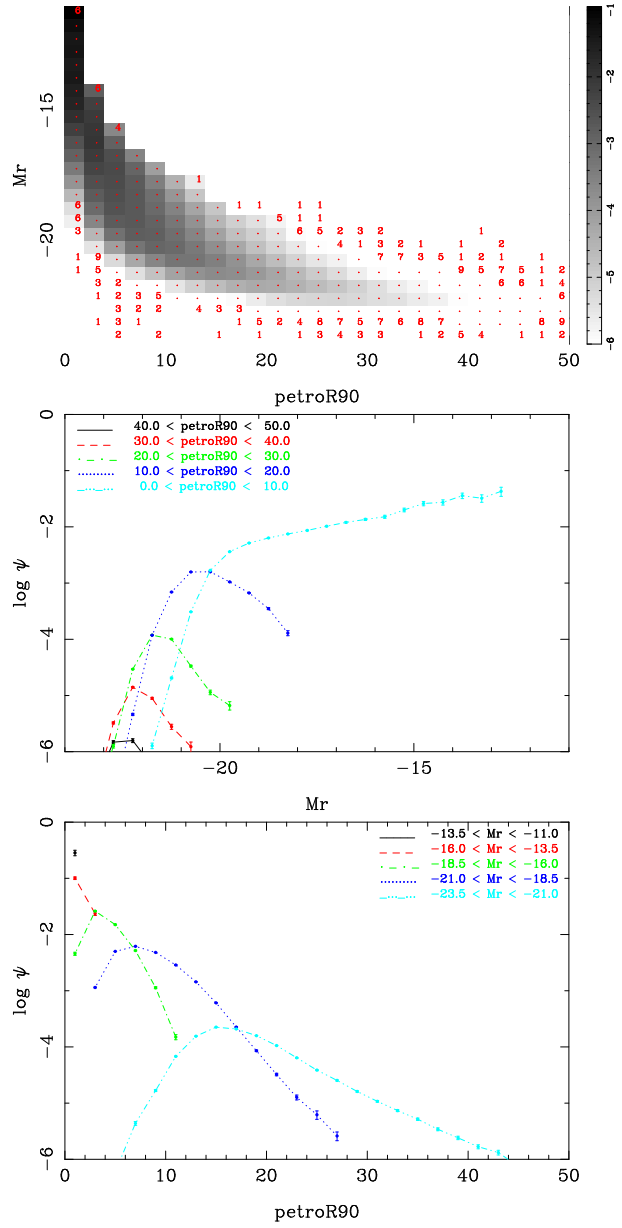


Figure 11. LF bivariate with absolute Petrosian 90% radius in kpc. The LF is Gaussian-like for all but the smallest radius, suggesting that the Schechter LF seen in other plots is due to the small galaxies in the respective samples.

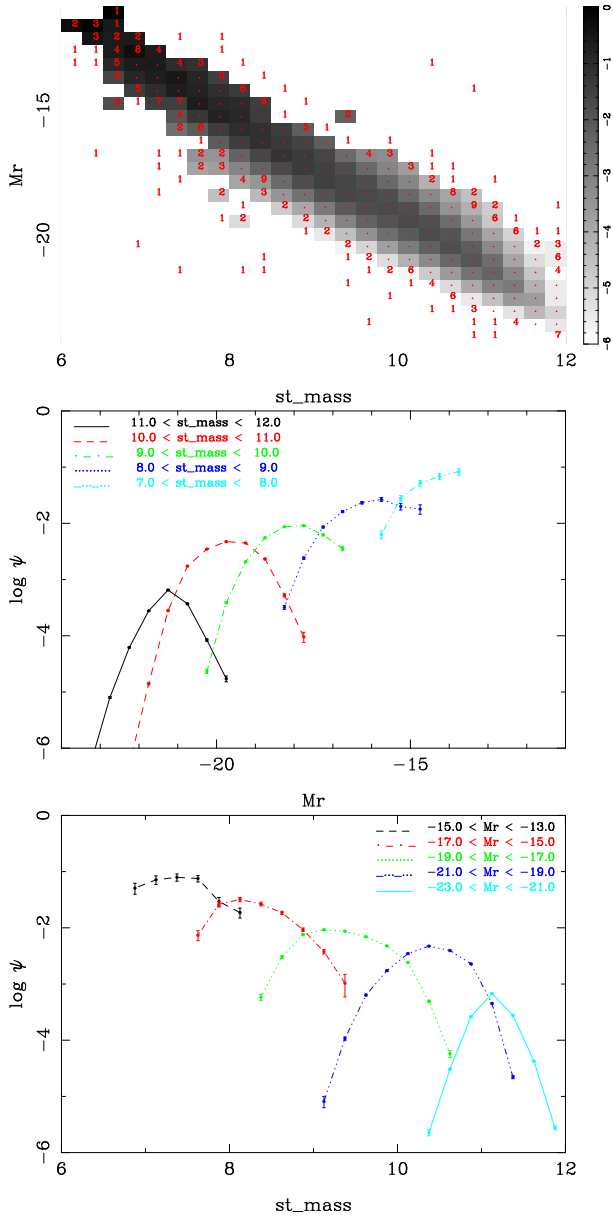


Figure 12. LF bivariate with galaxy stellar mass. Although the z band absolute magnitude correlates with stellar mass slightly more tightly than r , the r band is shown for consistency with the other LFs. The correlation is expected as the galaxy luminosity is used in the estimation of stellar mass.

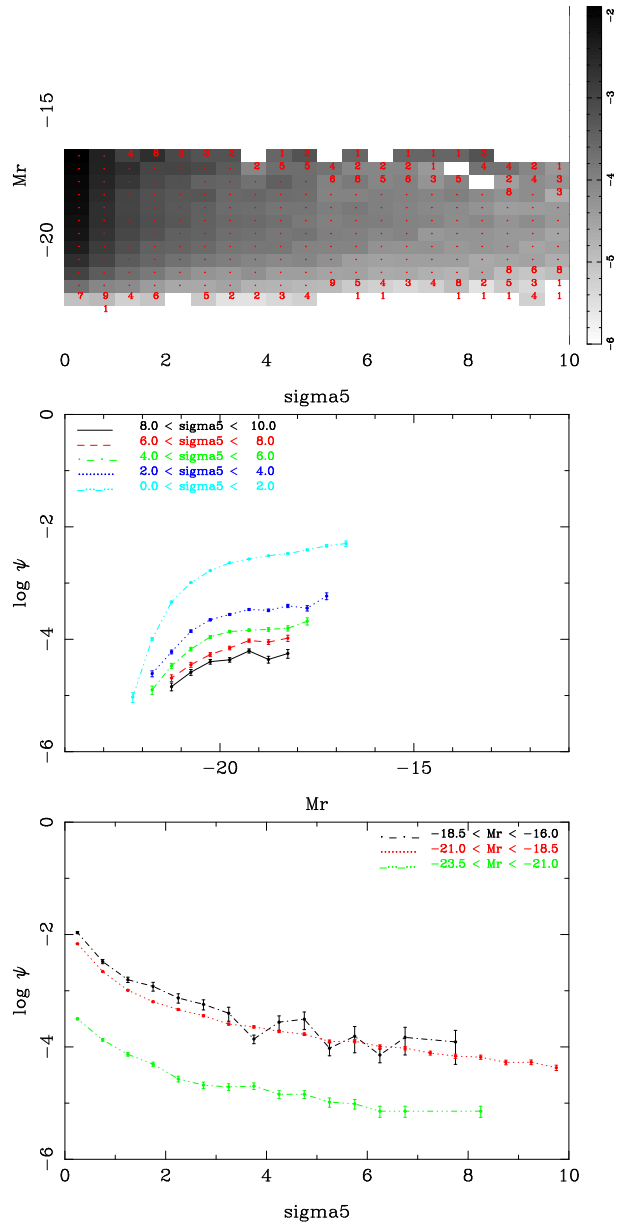


Figure 13. LF bivariate with Σ_5 surface density of galaxies. Unlike the other bivariate LFs here, the normalisation is arbitrary as it depends on the binning of the galaxies in density. The LF shape changes less dramatically than for the parameters shown previously.

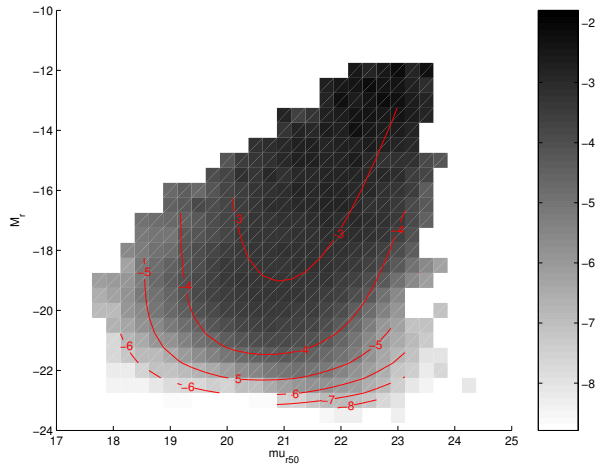


Figure 14. SWML estimate in greyscale and fitted Choloniewski function as contours for Petrosian half-light surface brightness. The right hand panel gives the LF $\log_{10} \psi$ value represented by the greyscale. The contours were fitted over the bins which contained five or more galaxies to minimise the effects of shot noise. The function provides a poor fit for bright galaxies.

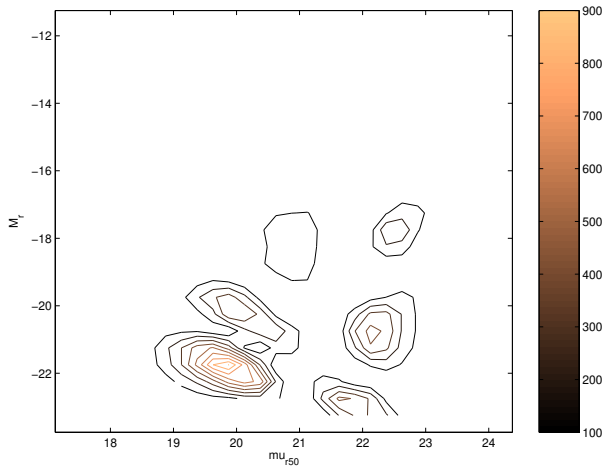


Figure 15. χ^2 values showing that the fit is generally poor, particularly for galaxies around $M_r = -22$ and $\mu_{R,50} = 20$. The right hand panel shows the χ^2 values represented by the contours.